Journal of Groundwater Science and Engineering 12(2024) 264–280

Journal homepage: http://gwse.iheg.org.cn

Research Paper

Application of hydrochemistry and strontium isotope for understanding the hydrochemical characteristics and genesis of strontium-rich groundwater in karst area, Gongcheng County, Southwest China

Mi Tang[1], Jun Lv[2], Shi Yu[1,3,4,5], Yan Liu[6], Shao-hong You[1,7*], Ping-ping Jiang[8*]

[1] *College of Environmental Science and Engineering*, *Guilin University of Technology*, *Guilin* 541004, *Guangxi*, *China*.
[2] *Guangxi Zhuang Autonomous Region Hydrographic Centre*, *Nanning* 530023, *China*.
[3] *Technical Innovation Center of Mine Geological Environmental Restoration Engineering in Southern Karst Area*, *Ministry of Natural Resources*, *Nanning* 530028, *China*.
[4] *Key Laboratory of Karst Dynamics*, *Ministry of Natural Resources & Guangxi Zhuang Autonomous Region*, *Institute of Karst Geology*, *Chinese Academy of Geological Sciences*, *Guilin* 541004, *Guangxi*, *China*.
[5] *International Research Centre on Karst under the Auspices of UNESCO/National Center for International Research on Karst Dynamic System and Global Change*, *Guilin* 541004, *Guangxi*, *China*.
[6] *Guilin Research Institute of Environmental Protection Sciences*, *Guilin* 541004, *Guangxi*, *China*.
[7] *Guangxi Key Laboratory of Green Preparation and Application of Inorganic Materials*, *Laibin* 546199, *Guangxi*, *China*.
[8] *College of Earth Sciences*, *Guilin University of Technology*, *Guilin* 541004, *Guangxi*, *China*.

Abstract: Understanding the hydrochemical characteristics and genesis mechanisms of strontium-rich groundwater is pivotal for supporting the exploitation and utilization of natural strontium-rich groundwater. In this research, 27 groundwater samples were collected. By analyzing major ion chemistry and strontium isotope data, and considering the hydrogeological context, various analytical approaches, including multivariate statistics, ion ratios, and isotopes, were used to reveal the characteristics and genesis mechanisms of strontium-rich groundwater in the study area. The findings indicate that the predominant hydrochemical type of groundwater is HCO_3-Ca, with Ca^{2+} and HCO_3^- as the primary cations and anions. The hydrochemistry of the strontium-rich groundwater is predominantly influenced by rock weathering processes. A combination of factors, including ion exchange, and anthropogenic activities, shapes the compositional characteristics of the groundwater in the region. The dissolution of calcite due to weathering emerges as the principal source of strontium in the groundwater. While ion exchange processes are not conducive to strontium enrichment in groundwater, their effect is relatively limited. The impact of human activities on the groundwater is minor.

Keywords: Hydrochemistry analysis; Strontium; $^{87}Sr/^{86}Sr$; Groundwater; Karst

Received: 15 Nov 2023/ Accepted: 18 May 2024/ Published: 10 Aug 2024

Introduction

Strontium is a necessary trace elements for the human body, which has important biological significance and toxicological significance for the physiological functions in human beings and other animals. It plays an indispensable role in bone growth and has certain therapeutic effects on the prevention and treatment of cardiovascular diseases (Marie et al. 2001; Kolodziejska et al. 2021). Strontium rich groundwater, as a type of natural mineral water, possesses the characteristics of recoverability, mobility and stable dynamic, and is increasingly popular among people. The exploration and exploitation of groundwater rich in strontium can provide additional alternatives for drinking water supply, meeting consumers' de-

*Corresponding author: Shao-hong You, Ping-ping Jiang, *E-mail address*: youshaohong@glut.edu.cn, jiangpp@glut.edu.cn

DOI: 10.26599/JGSE.2024.9280020

Tang M, Lv J, Yu S, et al. 2024. Application of hydrochemistry and strontium isotope for understanding the hydrochemical characteristics and genesis of strontium-rich groundwater in karst area, Gongcheng County, Southwest China. Journal of Groundwater Science and Engineering, 12(3): 264-280.

mand for healthy, high-quality drinking water. However, blindly exploiting strontium-rich groundwater not only wastes resources but also risks irreversible damage to the ecological environment. Thus, understanding the characteristics and formation mechanisms of strontium-rich groundwater is essential as a prerequisite for its sustainable development and utilization.

The formation of strontium-rich groundwater is influenced by various factors such as geological structure, hydrogeological conditions, and human activities. Evidence shows that the mineralogy and chemistry of rocks significantly control the composition of dissolved components in water bodies (Apollaro et al. 2007). From another perspective, the hydrochemical composition effectively records information about the geological setting of the watershed (Wang et al. 2001; Sun et al. 2023; Musgrove 2021), reflecting the geological and hydrogeological conditions of the study area. Consequently, analyzing groundwater hydrochemical parameters becomes a valuable tool for understanding the formation, controlling factors, and spatiotemporal distribution characteristics of groundwater. Researchers have employed various techniques to investigate strontium-rich groundwater. For instance, Cary et al. (2014) traced recharge sources and selenium origins of the Cretaceous aquifer in northern France using Ca/Sr, Mg/Sr, and Se/Sr ratios, along with strontium isotopes. Lebid et al. (2016) studied the contribution of strontium to groundwater salinity in the plains of northwestern Algeria. Simultaneously, combined with the analysis of strontium isotopes, valuable information about groundwater in complex terrain areas can be obtained. For instance, Baublys et al. (2019) explored the evolution of water from atmospheric precipitation to methane-rich groundwater using strontium isotopes. Huang and Ma (2019) revealed the evolution of the chemical components of groundwater in their study area, identifying water-rock interactions in carbonate or silicate rocks through major ion chemistry and C isotopes along with Sr isotopes. Gamboa et al. (2019) determined groundwater solute sources in the hyper-arid core of the Atacama Desert using major ions and multi-isotope compositions ($^{87}Sr/^{86}Sr$, $\delta^{34}S$, and $\delta^{18}O$). Strontium isotopes have also been used to reveal flow and hydraulic connections between two aquifers (Raiber et al. 2009; Santoni et al. 2016). Overall, significant advances have been made in understanding the origins and controlling factors of strontium in groundwater, the geochemical characteristics of Sr-rich groundwater, and the isotopic features of Sr-rich groundwater.

Gongcheng County, located southeast of Guilin, with a wide distribution of karst landform, characterized by underground rivers, caves and others. The Gongcheng River Basin serves as the primary production and living area in the study region, benefiting from abundant karst groundwater resources which constitute a vital water resources of the area. During regional geological surveys, several Sr-rich groundwater sites were identified, with strontium content greater than 0.2 mg/L, meeting the national standard for strontium content in natural mineral water for drinking (China standard GB 8537-2018). These sites hold significant potential for exploitation, yet the geochemical characteristics and formation mechanisms of strontium in karst groundwater remain unclear. To address this knowledge gap, various hydrogeochemical indices along with strontium isotope were used to identify hydrochemical characteristics and genesis of strontium-rich groundwater in karst area. It is expected that these findings will provide valuable guidance for the sustainable exploitation of strontium-rich groundwater in the study region.

1 Study area

Gongcheng County, located in the northeastern part of the Guangxi Zhuang Autonomous Region, features a topography that is higher in the north and lower in the south. The east and west sides exhibit significant uplifts, dominated by central steep slope terrain. Elevations in this area range from 123 m to 1,794 m, with relative height differences of 600–1,000 m or more. The central part of the study area is lower, forming a narrow north-south basin belt stretching from Limu to Gongcheng (Fig. 1a). This belt, which is 4 km to 5 km wide, consists of hills and isolated peak plains with elevations ranging from 150–500 m (Fig. 1b and Fig. 1c). The study area experiences a subtropical monsoon climate with abundant rainfall. Rainfall is concentrated between April and September (the period of abundant water), accounting for 64% of the total annual rainfall. The average annual rainfall is 1,382.1 mm. Additionally, the average temperature is 19.7°C, with the horizontal distribution of temperature affected by factors such as geographical latitude, elevation, and topography, resulting in higher temperatures in the south and lower temperatures in the north. The surface water system in the study area is well-developed, with the Xiling River in the west and the Gongcheng River in the center. Both rivers flow parallel from north to south through the entire region, with the

Gongcheng River Basin being the most extensive (Fig. 1a).

The study area is characterized by well-developed karst landforms, including peak-cluster depressions, isolated peak plains, and karst hill depressions. The study area is divided into three major categories of groundwater: Loose rock pore water, bedrock fissure water and karst water. Bedrock fissure water is primarily found in the structural, interlayer, and weathered fissures of clastic and intrusive rocks. Karst water is further divided into carbonate rock fissure cave water and carbonate rock-clastic rock fracture-cave water. There are two types of carbonate rock fissure cave water: Covered and exposed. While loose rock pore water is present in the pores of Quaternary loose rocks, and it's distribution is mainly associated with carbonate rock fissure cave water. The main aquifers in the study area consist of karst and fissured Cambrian carbonate rocks as well as Ordovician carbonate rocks (Fig. 1a).

The study region receives abundant atmospheric precipitation as a steady supply of groundwater recharge. For carbonate rock water-bearing formations, the rainfall infiltration coefficient ranges from 0.290 to 0.540. Groundwater collects from the higher terrain on the east and west sides of the mountains and flow towards the central lower terrain, eventually discharging into the Gongcheng River. Throughout the bottom mountainous regions with high terrain on both sides, number of surface streams with an east-west distribution are formed. These streams are replenished by both surface and groundwater from the bedrock mountainous areas and flow into the center covered karst area. Here, a layer of Quaternary soil (approximately 10 m to 20 m thick) covers the top layer of carbonate rock. Through this top soil layer, creek water and atmospheric rainfall from the clastic rock areas on both sides swiftly seep into the earth. The primary discharge pathways for karst water include rivers, springs, and artificial exploitation.

2 Samples and methods

In May 2021, a total of 14 karst groundwater samples and 13 $^{87}Sr/^{86}Sr$ isotope samples were systematically collected, including 4 pore groundwater, 5 fissure groundwaters and 5 karst groundwater. Karst groundwater was collected from the Upper Devonian and Lower Carboniferous limestone aquifers (Table 1). The sampling locations are depicted in Fig. 1a. During sample collection, a portable multi-parameter water quality analyzer

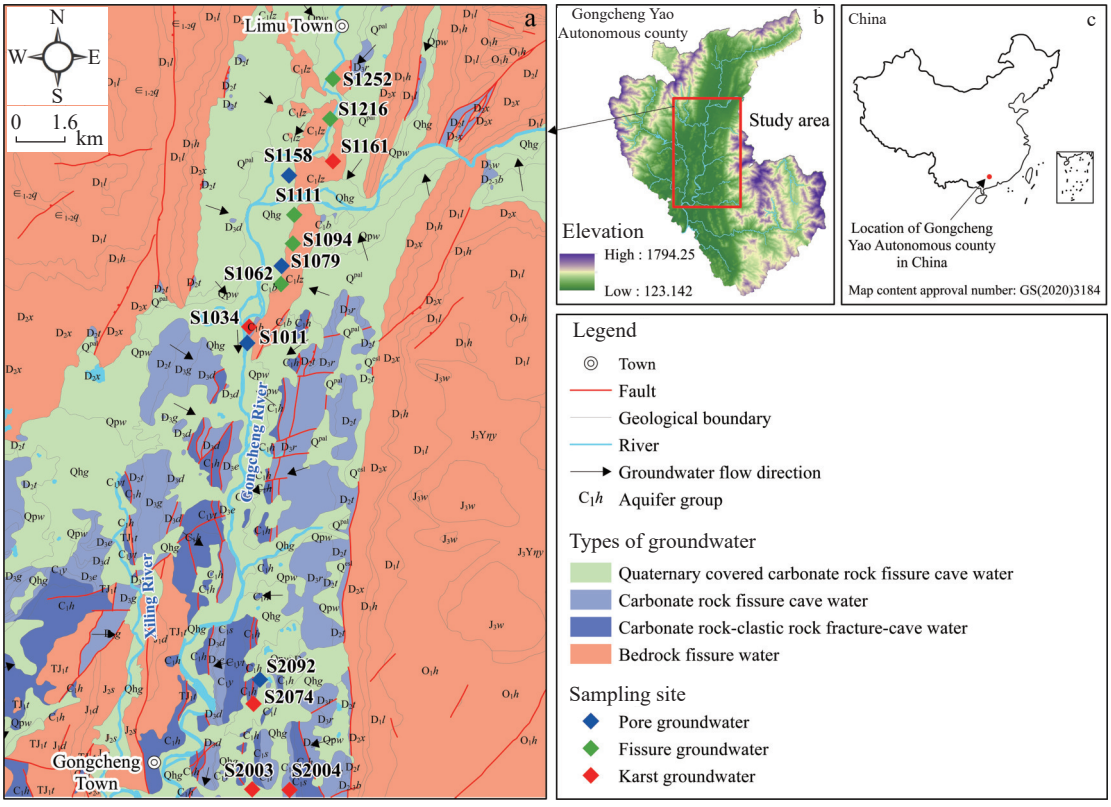

Fig. 1 (a) Simplified hydrogeological map of study area; (b) Elevation of study area; (c) Location of study area in China

Table 1 Statistical table of sampling groundwater from different aquifer

Groundwater type	Sampling site code	Sampling site	Depth of water table/m	Aquifer group	pH	Ec μs/cm	T /°C
Pore groundwater	S1158	well	2.5	Qhg	7.0	596	20.0
	S1079	well	0.3	Qhg	6.5	218	20.4
	S1011	well	6	Qhg	7.2	564	21.5
	S2092	spring	null	Op*w*	7.3	444	21.4
Fissure groundwater	S1111	motor-pumped well	0.9	C_1lz	7.1	354	25.5
	S1252	well	0.6	C_1lz	6.7	383	20.4
	S1216	spring	null	C_1lz	7.1	365	21.2
	S1094	spring	null	C_1lz	6.8	210	21.4
	S1062	spring	null	C_1lz	7.2	267	19.6
Karst groundwater	S1161	motor-pumped well	7.6	D_3r	6.6	96	21.8
	S1034	well	2	C_1b	6.8	408	22.8
	S2003	well	1.8	C_1h	7.3	474	23.0
	S2004	spring	null	C_1h	7.1	439	19.4
	S2074	spring	null	C_1h	7.2	252	23.5

(HQ40d, Hach, USA) was used to measure in-situ water temperature, Electrical Conductivity (EC), and pH. Additionally, cation concentrations K^+, Na^+, Ca^{2+} and Mg^{2+} were determined using Atomic Absorption Spectroscopy (AAS), while anion concentrations of the Cl^-, SO_4^{2-}, HCO_3^- and NO_3^- were measured using High-performance Liquid Chromatography (HPLC). Sr was determined using an Inductively Coupled Plasma Mass Spectrometer (ICP-MS). All tests were completed by the Test Center of Institute of Karst Geology, Chinese Academy of Geological Sciences. Strontium isotope ratios were measured using an isotope mass spectrometer (MAT-261) produced by Finnigan Mat in Germany and tested by the Wuhan Geological Survey Center of the China Geological Survey. The measured $^{87}Sr/^{86}Sr$ ratios were normalized to an $^{87}Sr/^{86}Sr$ value of 0.1194. During this study, the NBS987 Sr standard yielded 0.710248 ± 0.000029 (2σ, n = 20). Uncertainties on individual $^{87}Sr/^{86}Sr$ measurements were 8×10^{-6}. Data processing and analysis, including correlation analysis, factor analysis, and difference analysis, were performed using Excel and SPSS Statistics 20. Graphical processing was carried out using ArcGIS 10.2 and Origin 2021.

3 Results

3.1 Hydrochemical characteristics

In-situ parameters such as pH, EC, and temperature were measured for the Gongcheng groundwater samples (Table 1). The measured temperature ranged from 19.4°C to 25.5°C, which is higher than the annual average temperature of 19.7°C for the region. EC values ranged between 96 μs/cm and 596 μs/cm, while the pH of groundwater ranged from 6.5 to 7.3.

Analytical data for major ions in groundwater samples from the study area are presented in Table 2 and Fig. 2. The key findings are given below:

Cations in the groundwater samples were dominated by Ca^{2+}, while the concentrations of K^+, Na^+, and Mg^{2+} were generally low. Approximately half of the samples exhibited higher Ca^{2+} concentrations above 70 mg/L (Fig. 2a). The highest Ca^{2+} concentration was 116.20 mg/L at site S1011, while the lowest was 13.76 mg/L at site S1161. The median Ca^{2+} concentration in pore groundwater, fissure groundwater, and karst groundwater were 89.48 mg/L, 51.28 mg/L and 65.24 mg/L, respectively.

Anions in the groundwater samples were dominated by HCO_3^-. About half of the samples had higher HCO_3^- concentrations above 200 mg/L (Fig. 2b), followed by SO_4^{2-}, while the Cl^- concentrations were relatively low. The median HCO_3^- concentrations in pore groundwater, fissure groundwater, and karst groundwater were 249.72 mg/L, 164.40 mg/L and 216.42 mg/L, respectively, which are consistent with Ca^{2+}.

The NO_3^- concentrations in the groundwater varied significantly. The minimum concentration was less than 0.05 mg/L, while the maximum concentration reached 33.88 mg/L at sampling site S1252. In addition, the NO_3^- concentrations in the groundwater samples from sites S2092 and S2003 were 25.84 mg/L and 23.29 mg/L, respectively,

Table 2 Descriptive statistics of the main chemical components of groundwater

Parameters		TDS	K^+	Na^+	Ca^{2+}	Mg^{2+}	HCO_3^-	Cl^-	SO_4^{2-}	NO_3^-
		mg/L	mg/L	mg/L	mg/L	mg/L	mg/L	mg/L	mg/L	mg/L
Pore Groundwater (n=4)	Max.	256.80	8.46	16.79	116.20	9.47	368.34	24.74	53.86	25.84
	Min.	51.60	0.36	1.66	38.34	1.70	116.54	2.50	4.56	0.05
	Mean	151.62	3.47	5.91	83.37	4.18	246.08	10.03	18.60	8.04
	MD	149.04	2.52	2.60	89.48	2.78	249.72	6.44	8.00	3.13
Fissure groundwater (n=5)	Max.	225.7	6.22	3.42	78.03	4.16	214.34	8.71	29.35	33.88
	Min.	34.9	0.18	0.6	44.21	1.38	108.21	0.76	2.72	0.05
	Mean	103.48	1.81	1.50	57.74	3.15	168.14	3.75	12.93	9.54
	MD	103.48	0.4	1.12	51.28	3.39	164.4	2.18	8.91	2.42
Karst groundwater (n=5)	Max.	318.70	7.70	7.39	88.30	7.37	283.02	10.78	24.81	23.29
	Min.	215.30	0.19	0.42	13.76	0.74	24.97	1.16	5.98	0.05
	Mean	259.56	3.57	3.25	59.53	4.30	181.88	4.39	13.49	11.75
	MD	252.40	1.67	1.37	65.24	5.50	216.42	2.58	9.02	16.99

Note: Max.: maximum, Min.: minimum, MD: Median, TDS: Total dissolve solids.

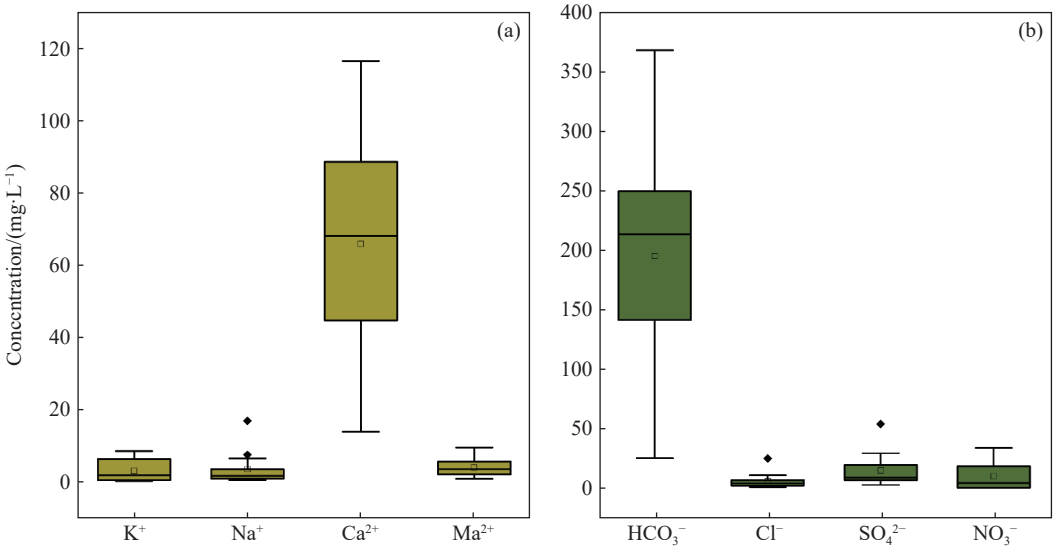

Fig. 2 The box diagram of (a) major cation content (K^+, Na^+, Ca^{2+}, Mg^{2+}) and (b) major anion content (HCO_3^-, Cl^-, SO_4^{2-}, NO_3^-) of groundwater

both exceeding 20 mg/L. These values are lower than the maximum NO_3^- concentration recommended by the World Health Organization guidelines (50 mg/L) but higher than the Chinese standards (20 mg/L).

The groundwater TDS (total dissolve solids) concentrations in the study area ranged from 34.9 mg/L to 318.70 mg/L, indicating low salinity freshwater. Karst groundwater had TDS values between 215.30 mg/L and 318.70 mg/L, with an average of 259.56 mg/L and a median concentration of 252.40 mg/L (higher than the other two types). The pore groundwater TDS ranged from 51.60 mg/L to 256.80 mg/L, while fissure groundwater TDS varied from 34.9 mg/L to 225.7 mg/L, both showing a wide range of variation.

Overall, the cation concentrations in karst groundwater followed this order: $Ca^{2+} > Mg^{2+} > Na^+ > K^+$, while the anion concentrations exhibit the following order: $HCO_3^- > SO_4^{2-} > NO_3^- > Cl^-$.

Based on the hydrochemical data, the percentage of Na^+, K^+, Ca^{2+}, Mg^{2+} in the total cation milliequivalents and the percentage of Cl^-, SO_4^{2-}, HCO_3^- in the total anion milliequivalents were calculated for each water sample. A Piper's trilinear diagram was then plotted for the water samples in the study area (Fig. 3). As shown in the figure, groundwater samples from the study area primarily fall into zones 4, A, and E of the diagram, indicating that the percentage of alkaline earth metal

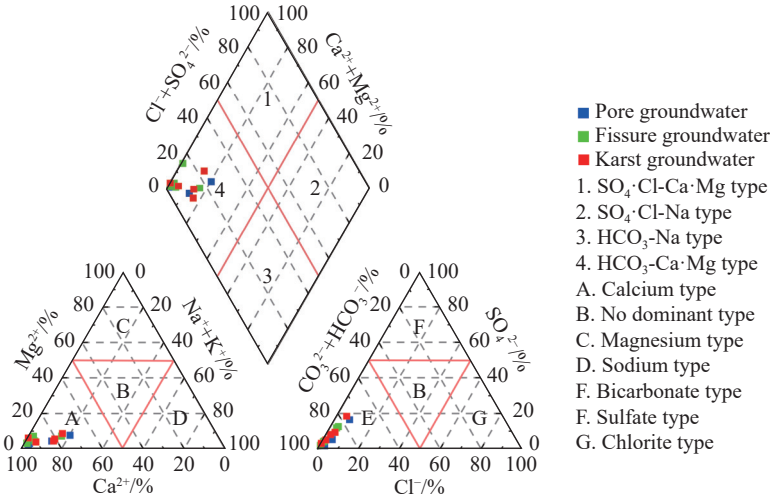

Fig. 3 Piper's trilinear diagram showing the hydrochemical facies of groundwater

ions (Ca^{2+}, Mg^{2+}) in milliequivalents exceeds that of alkali metal ions (Na^{+}, K^{+}), and the percentage of weak acid anions (HCO_3^-) exceeds that of strong acid anions (Cl^-, SO_4^{2-}), and carbonate hardness was more than 50%. Sr-rich groundwater falls into zones A and E of the Piper diagram, indicating that Ca^{2+} is the dominant cation and HCO_3^- is the primary anion in the groundwater samples. The groundwater in the study area exhibits chemical homogeneity, with HCO_3-Ca type being the predominant hydrochemical type. The TIS diagram provides information about the salinity of groundwaters, which is convenient to refer to the correlation diagram SO_4^{2-} vs. $HCO_3^- + Cl^-$ (Apollaro et al. 2019; Resz et al. 2023). The TIS diagram indicates that all samples have low Total Ionic Salinity (TIS) values, falling below the 16 meq/L iso-salinity line (Fig. 4).

A correlation analysis of hydrochemical components in groundwater can help explore the degree of correlation between major ions. This analysis provides a reference for revealing and identifying potential sources of solute components in groundwater (Esmaeili-Vardanjani et al. 2016; Chen et al. 2022; Liang et al. 2022). The correlation matrix of hydrochemical parameters in karst groundwater is shown in Table 3. Notably, HCO_3^- and Ca^{2+} exhibited a highly significant correlation with a coefficient of 0.982, indicating that carbonate rocks influence the water chemistry components in groundwater. Additionally, Cl^- showed a highly significant correlation with K^+ and Na^+, with correlation coefficients of 0.662 and 0.928, respectively. It also exhibited a significant correlation with Mg^{2+}, with a correlation coefficient of 0.661. Furthermore, SO_4^{2-} demonstrated highly significant correlations with K^+, Na^+, Mg^{2+}, with correlation coefficients of 0.672, 0.866, and 0.760, respectively. Besides, SO_4^{2-} and Cl^- showed highly significant correlation with correlation coefficients of 0.925, suggesting a common origin for both. However, the correlation coefficients between SO_4^{2-} and NO_3^- were insignificant, indicating that these two ions did not share a common source.

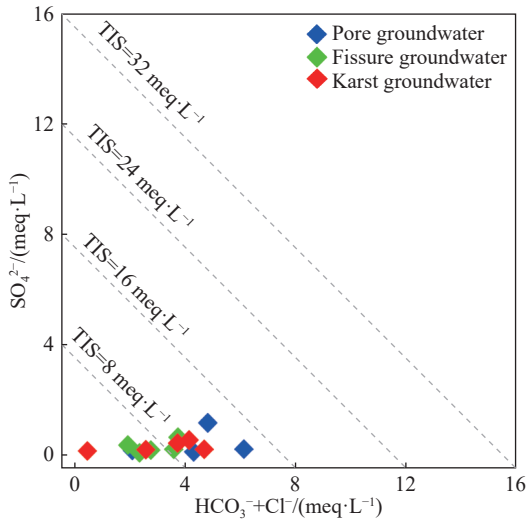

Fig. 4 Diagram of SO_4^{2-} vs. $HCO_3^- + Cl^-$ of groundwaters. Iso-salinity lines are drawn for reference

The correlation coefficient between Sr and Ca^{2+} in the karst groundwater of the study area was 0.537 ($P < 0.05$). Sr exhibited a relatively high correlation with HCO_3^-, with a correlation coefficient of 0.484. However, there was no significant correlation between Sr and Cl^- or SO_4^{2-}, with correlation coefficients of 0.163 and 0.194, respectively. Additionally, Sr exhibited negative correlations with K^+, Na^+ and Mg^{2+}, with correlation coefficients of −0.392, −0.118 and −0.051, respectively, indicating that the concentration of Sr in the groundwater tended to decrease as the concentrations of K^+, Na^+ and Mg^{2+} increased. It is possible

Table 3 Correlation coefficients between hydrochemical parameters of groundwaters (n=14)

	Sr	K^+	Na^+	Ca^{2+}	Mg^{2+}	HCO_3^-	Cl^-	SO_4^{2-}	NO_3^-
Sr	1								
K^+	−.392	1							
Na^+	−.118	.831**	1						
Ca^{2+}	.537*	.074	.284	1					
Mg^{2+}	−.051	.732**	.796**	.469	1				
HCO_3^-	.484	.033	.216	.982**	.465	1			
Cl^-	.163	.662**	.928**	.338	.661*	.224	1		
SO_4^{2-}	.194	.672**	.866**	.354	.760**	.256	.925**	1	
NO_3^-	−.375	.383	.057	−.212	−.058	−.295	−.001	−.096	1

Note: * * Indigenous at 0.01 level (bilateral), * Indigenous at 0.05 level (bilateral).

that cation exchange processes have constrained the release of strontium from the rocks.

3.2 Strontium and $^{87}Sr/^{86}Sr$ ratio

Strontium concentrations in the groundwater samples ranged from 0.04 mg/L to 0.64 mg/L (Table 4), with an average of 0.26 mg/L. The lowest and highest values were observed at the sites S1161, S1111, respectively, both of which are motor-pumped wells. When considering various types of groundwater, it is evident that the concentration of strontium in pore groundwater remains consistent and shows minimal fluctuations. In contrast, strontium levels in fissure groundwater and karst groundwater exhibit considerable variability, which may be related to the spatial heterogeneity of karst regions. Additionally, the $^{87}Sr/^{86}Sr$ values of the groundwater samples show relatively great variation, ranging from 0.708190 (site S2092) to 0.712393 (site S1158). Specifically, different groundwater types show distinctive Sr concentrations and $^{87}Sr/^{86}Sr$ ratios. The main features are: (1) pore groundwater shows the highest $^{87}Sr/^{86}Sr$ ratios (0.710000) and high Sr concentrations (average 0.31 mg/L), (2) fissure groundwater exhibits the lowest $^{87}Sr/^{86}Sr$ ratios (average 0.708446) and highest Sr concentrations (average 0.33 mg/L), and (3) karst groundwater displays higher $^{87}Sr/^{86}Sr$ ratios (average 0.709831) and lowest Sr concentrations (average 0.16 mg/L).

4 Discussion

4.1 Water–rock interactions

The Gibbs diagram effectively categorizes hydrogeochemical origins into three distinct mechanisms: atmospheric precipitation, rock weathering and evaporation (Gibbs, 1970). Illustrated in Fig. 5, the $Na^+/(Na^+{+}Ca^{2+})$ and $Cl^-/(Cl^-{+}HCO_3^-)$ ratios of strontium-rich groundwater predominantly align with the left side of the diagram, clearly indicating a 'rock weathering' classification. This suggests that the geochemical development of groundwater in the study area is primarily governed by rock weathering processes. The correlations between Ca^{2+}/Na^+ and Mg^{2+}/Na^+ molar ratios are instrumental in assessing the relative influence of principal weathering types (namely, carbonate, silicate, and evaporite rock weathering) on the groundwater's chemical composition (Gaillardet et al. 1999). Fig. 6 reveals that groundwater predominantly positions between the carbonate and silicate rock endmembers, leaning closer to the carbonate rock weathering side, and distinctly distant from evaporite influences. This pattern indicates that the groundwater in the research area is primarily dictated by the dissolution processes of carbonate rock weathering, with a notable but lesser impact from silicate rock weathering, and minimal effects from evaporite rocks.

To further reveal the origin of solutes in ground-

Table 4 Sr concentrations and $^{87}Sr/^{86}Sr$ ratios of different groundwater types

Groundwater type	Sr (mg/L)		$^{87}Sr/^{86}Sr$ (2σ)	
	Range	Average	Range	Average
Pore groundwater	0.28–0.36	0.31	0.708190–0.712393	0.710000
Fissure groundwater	0.12–0.64	0.33	0.708339–0.709489	0.708446
Karst groundwater	0.04–0.34	0.16	0.708289–0.710818	0.709831

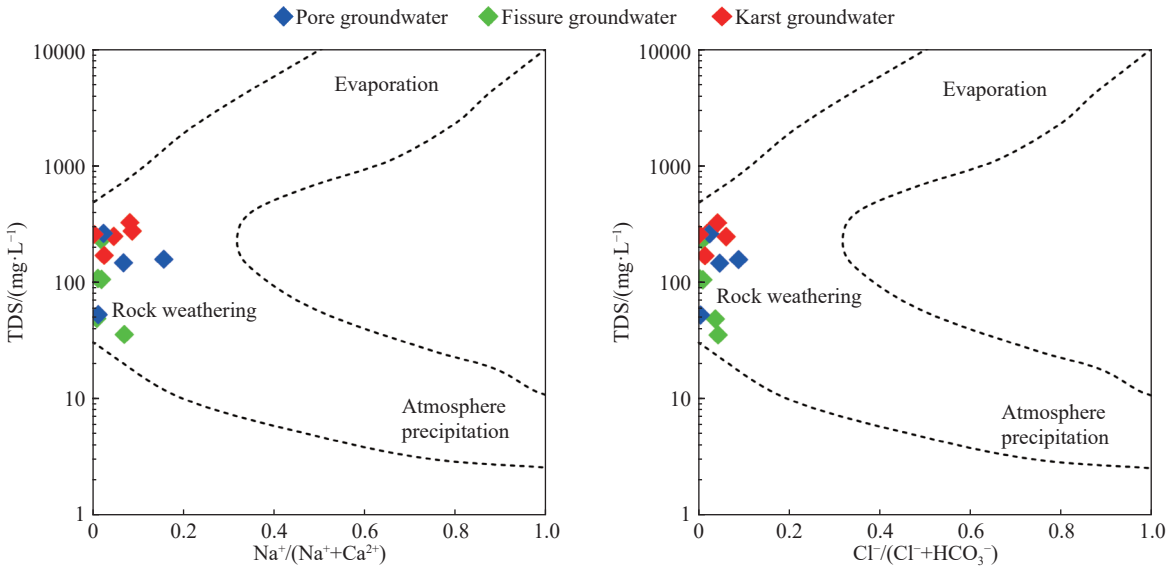

Fig. 5 Gibbs diagram of groundwater

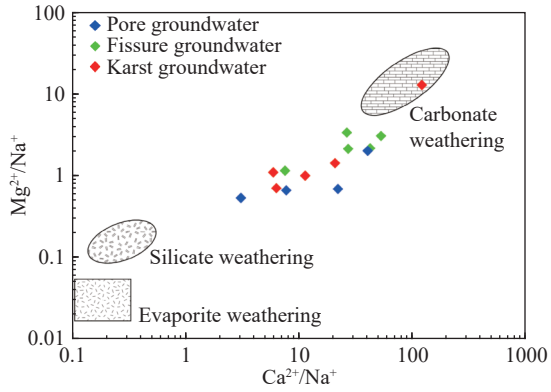

Fig. 6 Diagram of Ca^{2+}/Na^{+} vs. Mg^{2+}/Na^{+} of groundwater

water, ion ratio analysis between the dissolved chemical constituents is employed. Fig. 7a shows a considerably positive correlation (r^2 =0.68) between Ca^{2+}/Sr and Mg^{2+}/Sr molar ratios of groundwater from the study area, which suggests that Ca^{2+}, Mg^{2+}, and Sr in groundwater may share the same origin, indicating that the predominant source of dissolved Sr in groundwater is due to the dissolution of carbonate rocks. Furthermore, it is observed that all groundwater samples have higher Ca^{2+}/Sr molar ratios than Mg^{2+}/Sr molar ratios, with Ca^{2+}/Sr molar ratios ranging from 266.54 to 1,426.23 and Mg^{2+}/Sr molar ratios ranging from 15.60 to 265.64. Notably, Ph. Négrel et al. (Negrel and Petelet-Giraud 2005) studied the case of the Somme River and found that all groundwater samples from the Somme Basin plot similarly to rivers draining carbonate rock, with Ca/Sr and Mg/Sr ranging from 500 to 3,500 molar ratio and 25 to 150 molar ratio, respectively. Additionally, research by Zhang et al (Zhang et al. 2021) indicates that the molar ratios of Ca/Sr and Mg/Sr in the tributaries of the Xijiang River were 230.79 to 2,166.77, 122.06 to 500.34, respectively. The Gongcheng River, a secondary tributary of the Xi River,

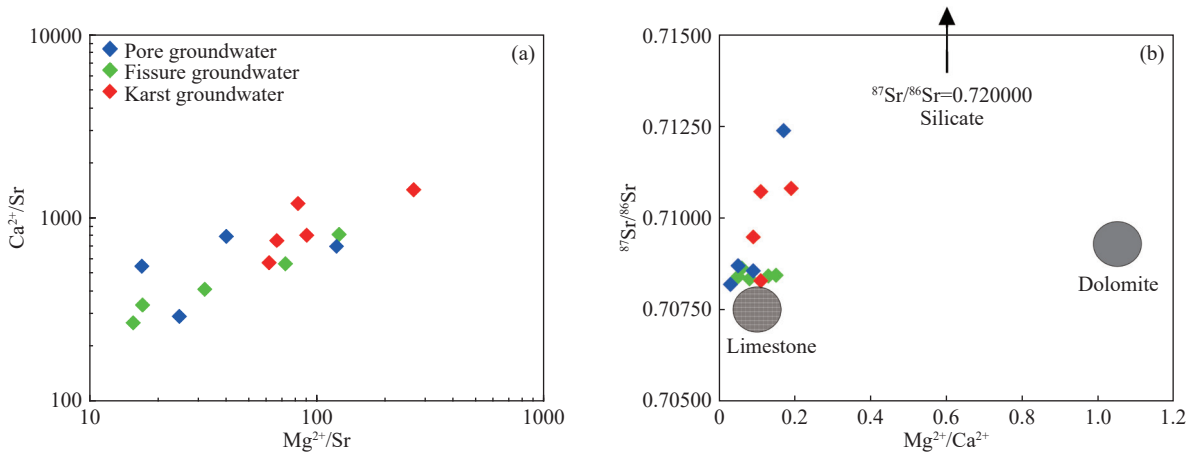

Fig. 7 Diagram of (a) Ca^{2+}/Sr vs. Mg^{2+}/Sr, (b) $^{87}Sr/^{86}Sr$ vs. Mg^{2+}/Ca^{2+} of groundwater

aligns with these patterns. Furthermore, they observed that limestone has much higher Ca/Sr molar ratios than Mg/Sr molar ratios, while dolomite's Ca/Sr molar ratios are almost consistent with its Mg/Sr molar ratios. Another case study by Pu et al. (2012) found that samples from dolomite aquifers display elevated Mg/Sr ratios, in contrast to those from limestone aquifers, which have lower Mg/Sr ratios. Consequently, considering the stratigraphic lithology of the study area, it is inferred that the dissolved Sr in the groundwater primarily originates from the dissolution of limestone.

Sr isotopes exhibit minimal fractionation in biological and chemical processes, making them valuable for tracing the source of substances and studying water-rock interactions and hydrogeochemical evolution in groundwater (Petelet-Giraud et al. 2003; Barbieri et al. 2005; Petelet-Giraud et al. 2007; Xie et al. 2013; Han and Eisenhauer 2021; Shoedarto et al. 2021). Sr primarily originates from the dissolution of silicate rock with high $^{87}Sr/^{86}Sr$ ratios, typically exceeding 0.7150 (Cartwright et al. 2007; Li et al. 2020), while Sr from limestone and dolomite dissolution have relatively low $^{87}Sr/^{86}Sr$ ratios, ranging from 0.7075 to 0.7080 and 0.7080 to 0.7100, respectively (He et al. 2022). Therefore, the relationship between Sr isotope ratios ($^{87}Sr/^{86}Sr$) and the Mg^{2+}/Ca^{2+} molar ratio can further be used to determine the dissolution of different minerals in groundwater (Li et al. 2010; Qin et al. 2017). The Sr isotopic compositions in different minerals are significantly different, with Sr originating from silicate rocks having high $^{87}Sr/^{86}Sr$ ratios, and moderate Mg^{2+}/Ca^{2+} molar ratios. Sr originating from carbonate rocks has low $^{87}Sr/^{86}Sr$ ratios, accompanied by low Mg^{2+}/Ca^{2+} molar ratios (0.01–0.26) in limestone aquifers and higher (0.085–1.07) in the dolomite aquifer (Pu et al. 2012). Thus, the average ratio of $^{87}Sr/^{86}Sr$ of 0.707500 and low Mg^{2+}/Ca^{2+} molar ratio (around 0.10), the average ratio of $^{87}Sr/^{86}Sr$ of 0.709300 and higher Mg^{2+}/Ca^{2+} value (about 1.05), as well as the average ratio of $^{87}Sr/^{86}Sr$ of 0.720000 and medium Mg^{2+}/Ca^{2+} value (about 0.70) can be taken as end members of dissolved limestone, dolomite and silicate rocks respectively. As shown in Fig.7b, the groundwater samples in the study area cluster near the dissolution characteristics of limestone, showing little proximity to dolomite. The molar ratio of Mg^{2+}/Ca^{2+} (0.03–0.19) aligns with the dissolution feature of the limestone aquifer. This result is consistent with the regional geological background. Specifically, the sampling sites in the study area are mainly located in the Gongcheng River Basin, characterized by karst landforms dominated by carbonate rocks (with calcite as the main mineral). Additionally, some samples (S1158, S1034, and S2003) exhibit a tendency toward the dissolution of silicate rocks, suggesting that a portion of the dissolved Sr in karst groundwater might originate from the weathering of silicate rocks.

Owing to the interactions between water and rock, the hydrochemical composition of groundwater tends to be intricate and diverse. Calculating the mineral saturation index helps identify whether water-rock interactions are dominated by dissolution or deposition. It also reflects the degree of saturation of dissolved minerals in the groundwater, allowing an evaluation of its dissolution capacity (Liu et al. 2023; Ullah et al. 2023). In this study, the hydrogeochemical modeling software PHREEQC was utilized to determine the saturation index (*SI*) for various minerals in the groundwater. As depicted in Fig. 8, while calcite and aragonite exhibit fluctuations near an *SI* of 0 in a few samples, the majority of minerals have significantly negative *SI* values, indicating a state of dissolution. These minerals could feasibly dissolve along the groundwater flow path (Yuan et al. 2017; Zhang et al. 2020). Additionally, a distinct overall correlation exists between the mineral *SI* and Sr concentration in the groundwater when the Sr concentration is below 0.3 mg/L. This suggests that the dissolution of these minerals contributes notably to the presence of dissolved strontium in the groundwater.

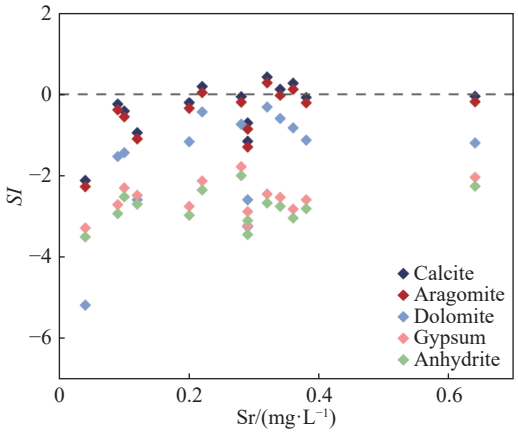

Fig. 8 Diagram of the Sr^{2+} and *SI* of different minerals of groundwater

Fig. 9a to Fig. 9e illustrate the relationship between the mineral Saturation Index (*SI*) and Total Dissolved Solids (TDS) across different groundwater types of study area. Overall, there is no significant correlation between groundwater TDS and the *SI* of various minerals. However,

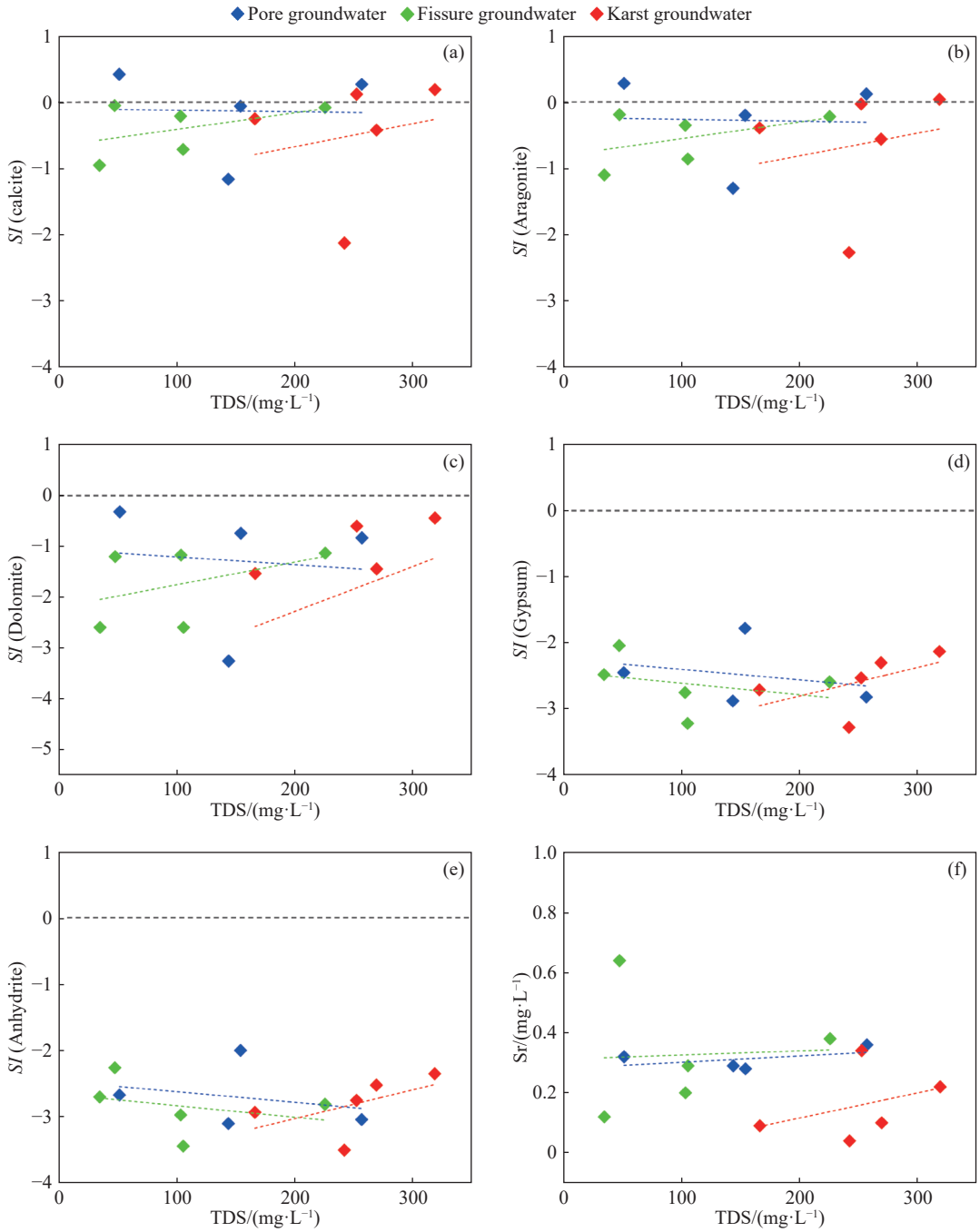

Fig. 9 Diagram of *SI* vs. TDS (a) calcite, (b) aragonite, (c) dolomite, (d) gypsum, and (e) anhydrite), (f) Sr vs. TDS of groundwater

when examining specific types, there appears to be a consistent negative correlation between TDS and the *SI* of minerals in the pore water, suggesting these minerals don't progressively dissolve along the groundwater's path. In the case of fissure water, a positive correlation emerges between the saturation indices of calcite, aragonite, and dolomite, and TDS, contrasting with the negative correlation observed for gypsum and anhydrite. This pattern suggests that the primary dissolution contributing to TDS in fissure water involves calcite, aragonite, and dolomite from the fissured aquifer. Conversely, karst waters show a positive correlation between the saturation indices of their minerals and TDS, with an increase in *SI* accompanying rising TDS. This pattern indicates ongoing interactions between karst groundwater and the soluble minerals in the aquifer. Fig. 9f further illustrates a notable correlation between Sr concentration and TDS in the area's groundwater. This suggests that groundwater along its flow path continuously leaches soluble minerals from the aquifer, releas-

ing and accumulating Sr in the aquifer (Yang et al. 2022). The study observes that Sr enrichment in karst waters is particularly influenced by water-rock interactions. It is generally believed that the longer groundwater remains within an aquifer and the more extensive its circulation path, the more likely it is for Sr to be released and enriched in the groundwater. This comprehensive analysis suggests that the concentration of dissolved strontium in the region's strontium-rich groundwater is influenced not only by rock weathering but also by other contributing factors.

4.2 Ion-exchange processes

Ion exchange is a key factor influencing the chemical composition of water and is commonly observed in groundwater environments. The graph depicting the milliequivalent concentration relationship between (Mg^{2+}+Ca^{2+}) - (SO_4^{2-} -HCO_3^-) and (Na^++K^+-Cl^-) serves as an indicator of ion exchange processes in groundwater (Lu et al. 2023). A ratio of −1 for these values signals the occurrence of such process. As illustrated in Fig. 10a, the majority of water samples clusters around the −1:1 ratio line, indicating that ion exchange reactions among Na^+, K^+, Ca^{2+}, and Mg^{2+} are taking place in the groundwater. The Chloro-Alkaline Index (CAI), introduced by Schoeller in 1967, provides a more detailed analysis of the type and intensity of ion exchange (Schoeller, 1967). The formula for its calculation is as follows:

$$\text{CAI 1} = \frac{Cl^- - (Na^+ + K^+)}{Cl^-} \quad (1)$$

$$\text{CAI 2} = \frac{Cl^- - (Na^+ + K^+)}{SO_4^{2-} + HCO_3^- + CO_3^{2-} + NO_3^-} \quad (2)$$

All ions are measured in equivalent concentrations in equation (1) and (2). As depicted in the chloro-alkaline index graph (Fig. 10b), most groundwater samples show negative values for both CAI1 and CAI2. This suggests that in the groundwater, Ca^{2+} and Mg^{2+} have undergone exchange reactions with Na^+ and K^+ present in the aquifer, resulting in the entry of Na^+ and K^+ into the groundwater. In the study area, the chloro-alkaline index values for groundwater primarily concentrate between −2 and 1 for CAI1 and between −0.01 and 0.05 for CAI2. The relatively modest absolute values of CAI1 and CAI2 indicate limited variation in the chloro-alkaline index values, suggesting that ion exchange processes in the

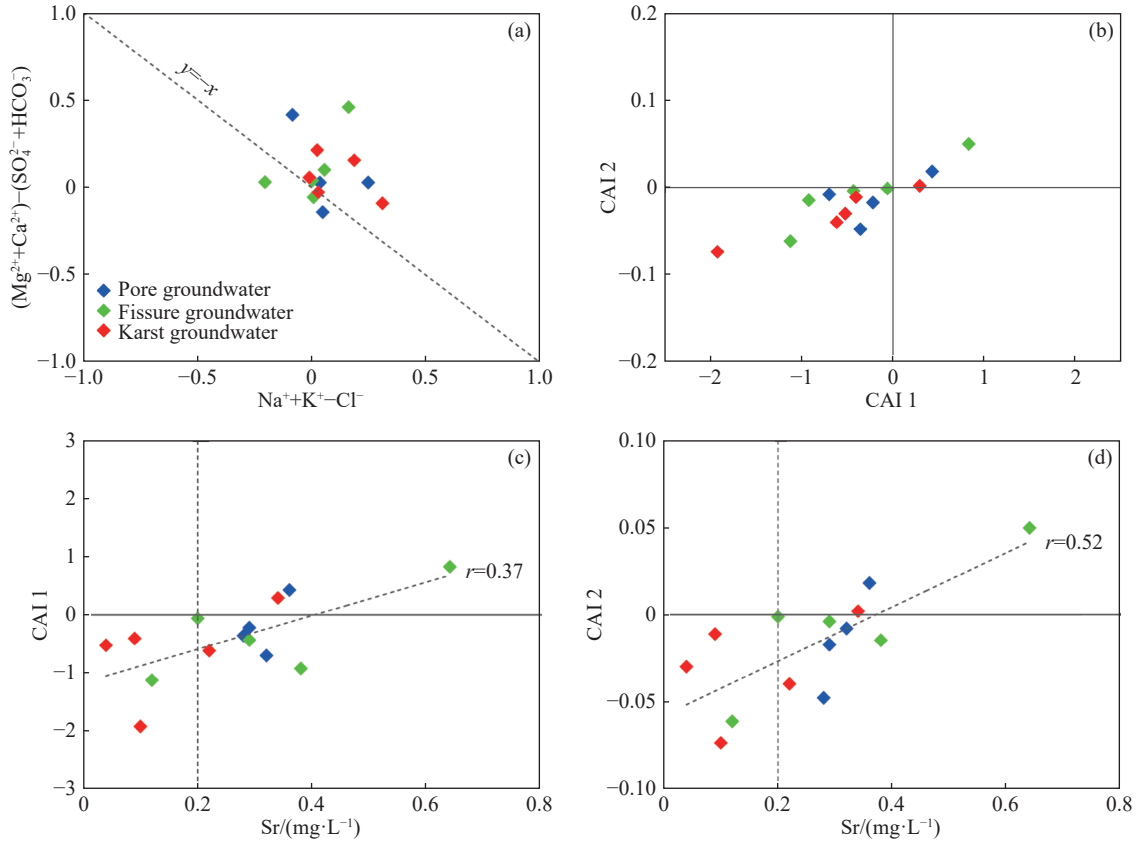

Fig. 10 Diagram of (a) $Na^+ + K^+ - Cl^-$ vs. (Mg^{2+}+ Ca^{2+}) – (SO_4^{2-} + HCO_3^-), (b) CAI 1 vs. CAI 2, (c) Sr vs. CAI 1, and (d) Sr vs. CAI 2 of groundwater

groundwater are not particularly intense (Wang et al. 2015). Fig. 10c and Fig. 10d illustrate a noticeable correlation between the chloro-alkaline index and the concentration of Sr in the groundwater. There is a trend where an increase in CAI1 and CAI2 values corresponds to an increase in the Sr content in the groundwater (or a decrease in Sr content with an increase in the absolute values of CAI1 and CAI2), implying that ion exchange has a certain impact on the enrichment of Sr in the groundwater, i.e., it is not conducive to the enrichment of strontium in the groundwater. This observation is consistent with the negative correlation found between Sr and K^+, Na^+ in the groundwater (Table 3). Furthermore, Fig.10c and Fig. 10d also show three points with positive values for both CAI1 and CAI2, namely S1111 (fissure water), S2092 (pore water), and S2004 (karst water). This implies that these three sampling sites are primarily undergoing reverse ion exchange, where Na^+ and K^+ in the groundwater exchange with Ca^{2+} and Mg^{2+} from the aquifer minerals, resulting in a decrease in Na^+ and K^+ and an increase in Ca^{2+} and Mg^{2+} in the groundwater. Notably, high concentrations of dissolved strontium were detected at these locations. Given the chemical similarity between Sr^{2+} and Ca^{2+}, Na^+ and K^+ might also displace Sr from the sediments into the groundwater in the reverse ion exchange process, thereby increasing the dissolved Sr content. Through the above analysis, it is evident that ion exchange significantly influences the Sr enrichment in the groundwater of the study area, and indicating that the primary source of Sr in the area's groundwater is derived from carbonate rocks.

4.3 Anthropogenic inputs to the groundwater

With the economic development, human activities (such as domestic sewage and agricultural activities) have also impacted the hydrochemical composition of groundwater (Böhlke and Horan 2000; Jiang et al. 2009; Christian et al. 2011; Zieliński et al. 2021). In natural groundwater, K^+ and Na^+ originate from various sources, including atmospheric precipitation, dissolution of salt (halite) rocks, weathering of silicate rocks and human activities (Xiao et al. 2014; Liu et al. 2022). Since the study area is far from the ocean, the contribution of K^+ and Na^+ from atmospheric precipitation is very low. In addition, considering the geological background of the study area, salt (halite) rocks are scarce, suggesting that atmospheric precipitation and salt (halite) rock dissolution are not the primary sources of K^+ and Na^+ in the groundwater. Silicate rock weathering can release K^+, Na^+ and Sr simultaneously. Therefore, the $Sr/[K^+ + Na^+]$ and $^{87}Sr/^{86}Sr$ ratios serve as useful tools for assessing the contribution of silicate rocks and human activities to Sr enrichment. Wu et al. (2014) used an inversion model to evaluate the impact of six end members, namely, rainfall, human activities (urban sewage and agricultural activities), evaporation, carbonate weathering, and silicate weathering on Sr sources in the Xi River Basin. The $^{87}Sr/^{86}Sr$ ratios were 0.7101–0.7102 and 0.707–0.709 for municipal wastewater and agricultural activities, respectively. Jiang et al. concluded that Sr from human sources (e.g. agricultural fertilizers and domestic wastewater or sewage) have $^{87}Sr/^{86}Sr$ ratios greater than 0.7080 (Jiang, 2011). It can be seen that the $^{87}Sr/^{86}Sr$ ratios influenced by human activities, particularly agricultural practices, are lower, approximately 0.708, in comparison to the ratios derived from silicate rock weathering, which ranges from 0.716 to 0.720 (Acharya et al. 2022). Moreover, groundwater impacted by human activities also exhibits notably lower $Sr/[K^+ + Na^+]$ ratios due to pollution from agricultural and domestic wastewater, resulting in elevated K^+ and Na^+ concentrations. In this study, as shown in Fig. 11, the karst groundwater sample are clearly divided into two parts. The samples concentrated on the right side of the figure have lower $^{87}Sr/^{86}Sr$ values and higher $Sr/[K^+ + Na^+]$ values, indicating that Sr in this group may originate from carbonate rock weathering, as it contains very little K^+ and Na^+. On the other hand, the samples concentrated on the left side of the figure exhibit two different trends. Samples (S1158, S1034, and S2003) have lower $Sr/[K^+ + Na^+]$ values and relatively high $^{87}Sr/^{86}Sr$ values, all exceeding 0.710000. These points may be affected by silicate rocks weathering. This finding aligns with the observations in Fig. 7b, indicating that these three points are closer to the endmember representing silicate rock weathering. The remaining samples have lower $Sr/[K^+ + Na^+]$ values and $^{87}Sr/^{86}Sr$ values. It is noteworthy that these samples display a marked variation in the $Sr/[K^+ + Na^+]$ ratio (spanning from 0.0044 to 0.0387), yet the $^{87}Sr/^{86}Sr$ ratio is relatively stable, ranging between 0.708190 and 0.708700. These samples likely reflect the influence of anthropogenic activities (mainly agricultural activities fertilizers, such as potash fertilizers, ammonium sulphate, and N/P/K fertilizer mixtures, etc., as well as discharge of sewage water from agricultural fields), affecting the K^+ and Na^+ concentra-

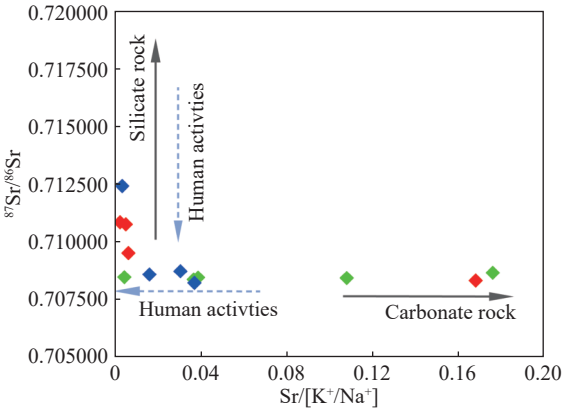

Fig. 11 Diagram of $^{87}Sr/^{86}Sr$ vs. Sr/[K^+ + Na^+] of groundwater

tion of in groundwater. Based on the above analysis, combined with the previously discussed correlation results, it is concluded that the concentration of Sr in groundwater demonstrates negligible correlations with K^+, Na^+, Cl^-, SO_4^{2-} and NO_3^-. In fact, there is even a negative correlation observed with Na^+, K^+, and NO_3^- (Table 3). This suggests that human activities have minimal impact on the Sr content in the groundwater.

The ion ratio coefficients of groundwater chemical compositions play a crucial role in understanding their origin and tracing the hydrochemical evolution process (Che et al. 2021). NO_3^- serves as a common indicator of groundwater contamination (Zhang et al. 2023). As shown in Table 2, a wide range in NO_3^- concentrations is observed across different groundwater sites, with values ranging from 0.05 mg/L to 33.88 mg/L. It's widely acknowledged that NO_3^- in groundwater primarily results from agricultural activities, as well as the influence of animal waste and human sewage (Su et al. 2023). Fig. 12a reveals that groundwater in the study area exhibits relatively small SO_4^{2-}/Ca^{2+} and NO_3^-/Ca^{2+} ratios, suggesting a slight impact from mining activities and agricultural activities. The analysis of NO_3^- sources using the NO_3^-/Cl^- ratio and Cl^- concentration (Fig. 12b) indicates that most groundwater samples align closely with the endmember associated with agricultural fertilizers, pointing to this as the principal source of NO_3^- in groundwater. Given the dense population engaged in agriculture along the Gongcheng River, the study area's groundwater is particularly susceptible to contamination from agricultural fertilizers.

Overall, with a few exceptions, the groundwater has been lightly impacted by human activity in study area, and the general degree of groundwater contamination is fairly low. In fact, there is an abundance of groundwater in the research area. While making sure that groundwater resources are protected, it is advised to increase the development and usage of strontium-rich groundwater resources in the area. Additionally, it is suggested to utilize groundwater that is rich in strontium since this might have positive effects on the environment and the economy.

5 Conclusions

This research employed various analytical methods, including hydrochemical parameters and strontium isotope analysis, to interpret the hydrochemical formation of groundwater in the study area. Perspectives such as rock weathering, mineral dissolution, ion exchange, and human activities were considered. These insights contribute to understanding the hydrochemical characteristics and genesis of strontium rich groundwater in karst area. Key findings of the study include:

(1) The hydrochemical composition of groundwater in the study area is influenced by various hydrogeochemical processes, including rock weath-

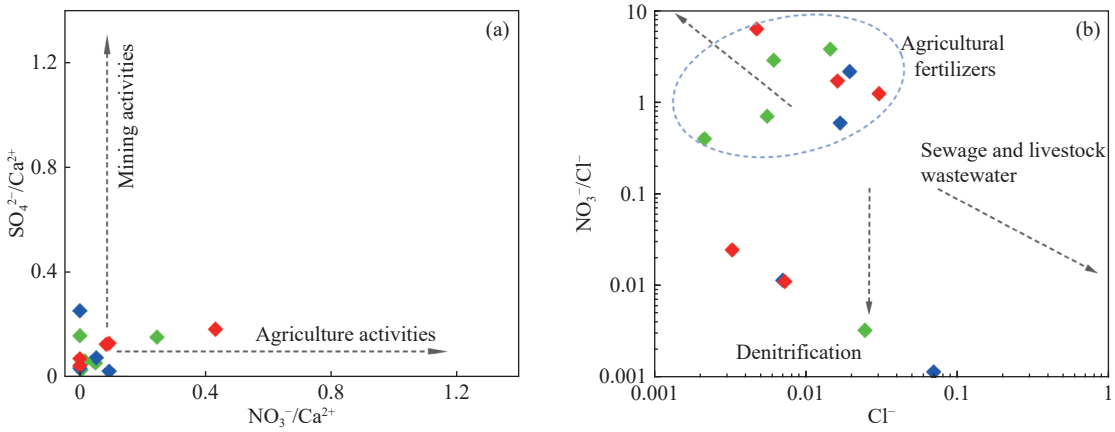

Fig. 12 Diagram of (a) SO_4^{2-}/Ca^{2+} vs. NO_3^-/Ca^{2+}, (b) NO_3^-/Cl^- vs. Cl^- of groundwater

ering, mineral dissolution, ion exchange, and anthropogenic inputs. The hydrochemistry of groundwater in the study area primarily manifests as HCO_3-Ca type. Ca^{2+} and HCO_3^- are the dominant cations and anions, respectively, largely governed by carbonate dissolution. The primary drivers controlling the hydrochemical formation of strontium-rich groundwater are rock weathering and mineral dissolution, with limited influence from ion exchange altering the hydrochemical composition.

(2) The study area features numerous strontium-rich water sites, with strontium concentrations in groundwater ranging from 0.04 mg/L to 0.64 mg/L, averaging at 0.26 mg/L. The interaction of groundwater with aquifer's rock minerals largely determined the strontium source. Calcite weathering dissolution emerges as the main contributor to groundwater's dissolved strontium. Ion exchange processes, however, do not conducive to strontium enrichment in groundwater.

(3) Human activities have relatively minor influence on groundwater in the study area. The region has been less contaminated, and there is an abundance of groundwater resources. Scientific exploration and utilization of strontium-rich groundwater could benefit the regional economy while safeguarding this valuable resource.

In summary, this research integrates hydrochemical and isotopic data to understand the influence of water-rock interactions and human activities on the hydrogeochemical environment of karst groundwater. The geological background plays a significant role in hydrochemical composition of strontium-rich groundwater in the study area. Moreover, this strontium-rich groundwater represents a valuable natural resource with considerable economic potential. The initial findings from this study provide a reference for the safeguarding and rational exploitation of strontium-rich groundwater resources in the study area.

Acknowledgement

This study was supported by the Guangxi Natural Science Foundation (2020GXNSFAA297025), the Guangxi Natural Science Foundation (GuikeAB2 2080046), the Guangxi Natural Science Foundation (GuikeAB21196050), the National Natural Science Foundation of China (42177075), the Natural Resources Science and Technology Strategic Research Project (2023-ZL-23), and the Survey and China Geological Survey (DD20221808 and DD20230547).

References

Acharya SS, Hishamunda V, Chakrabarti R. 2022. Natural sources and anthropogenic influences on the river water and groundwater chemistry of the lower Mahanadi Basin: Insights from radiogenic Sr isotopes and major ion chemistry. Frontiers in Water, 4: 846438. DOI：10.3389/frwa.2022.846438.

Apollaro C, Buccianti A, Vespasiano G, et al. 2019. Comparative geochemical study between the tap waters and the bottled mineral waters in Calabria (Southern Italy) by compositional data analysis (CoDA) developments. Applied Geochemistry, 107: 19−33. DOI：10.1016/j.apgeochem.2019.05.011.

Apollaro C, Marini L, De Rosa R, et al. 2007. Geochemical features of rocks, stream sediments, and soils of the Fiume Grande Valley (Calabria, Italy). Environmental Geology, 52(4): 719−729. DOI：10.1007/s00254-006-0508-6.

Barbieri M, Boschetti T, Petitta M, et al. 2005. Stable isotope (2H, 18O and 87Sr/86Sr) and hydrochemistry monitoring for groundwater hydrodynamics analysis in a Karst aquifer (Gran Sasso, Central Italy). Applied Geochemistry, 20(11): 2063−2081. DOI：10.1016/j.apgeochem.2005.07.008.

Baublys KA, Hamilton SK, Hofmann H, et al. 2019. A strontium ($^{87}Sr/^{86}Sr$) isotopic study on the chemical evolution and migration of groundwaters in a low-rank coal seam gas reservoir (Surat Basin, Australia). Applied Geochemistry, 101: 1−18. DOI：10.1016/j.apgeochem.2018.12.020.

Böhlke JK, Horan M. 2000. Strontium isotope geochemistry of groundwaters and streams affected by agriculture, Locust Grove, MD. Applied Geochemistry, 15(5): 599−609. DOI：10.1016/s0883-2927(99)00075-x.

Cartwright I, Weaver T, Petrides B. 2007. Controls on $^{87}Sr/^{86}Sr$ ratios of groundwater in silicate-dominated aquifers: SE Murray Basin, Australia. Chemical Geology, 246(1−2): 107−123. DOI：10.1016/j.chemgeo.2007.09.006.

Cary L, Benabderraziq H, Elkhattabi J, et al. 2014. Tracking selenium in the Chalk aquifer of northern France: Sr isotope constraints.

Applied Geochemistry, 48: 70−82. DOI：10.1016/j.apgeochem.2014.07.014.

Che QH, Su XS, Wang SX, et al. 2021. Hydrochemical characteristics and evolution of groundwater in the alluvial plain (anqing section) of the Lower Yangtze River Basin: Multivariate statistical and inversion model analyses. Water, 13(17): 2403. DOI：10.3390/w13172403.

Chen H, Wang JD, Zhang F, et al. 2022. Hydrochemical characteristics and formation mechanisms of groundwater in West Zoucheng City, Shandong Province, China. Environmental Monitoring and Assessment, 194(8): 573. DOI：10.1007/s10661-022-10136-2.

Christian LN, Banner JL, Mack LE. 2011. Sr isotopes as tracers of anthropogenic influences on stream water in the Austin, Texas, area. Chemical Geology, 282(3−4): 84−97. DOI: 10.1016/j.chemgeo.2011.01.011.

Esmaeili-Vardanjani M, Rasa I, Yazdi M, et al. 2016. The hydrochemical assessment of groundwater resources in the Kadkan Basin, Northeast of Iran. Carbonates and Evaporites, 31(2): 129−138. DOI：10.1007/s13146-015-0248-3.

Gaillardet J, Dupré B, Louvat P, et al. 1999. Global silicate weathering and CO_2 consumption rates deduced from the chemistry of large rivers. Chemical Geology, 159(1−4): 3−30. DOI: 10.1016/s0009-2541(99)00031-5.

Gamboa C, Godfrey L, Herrera C, et al. 2019. The origin of solutes in groundwater in a hyperarid environment: A chemical and multiisotope approach in the Atacama Desert, Chile. Science of the Total Environment, 690: 329−351. DOI：10.1016/j.scitotenv.2019.06.356.

Gibbs RJ. 1970. Mechanisms controlling world water chemistry. Science, 170(3962): 1088−1090. DOI：10.1126/science.170.3962.1088.

Han GL, Eisenhauer A. 2021. Stable and radiogenic strontium isotope cycling in a representative Karst forest ecosystem, Southwest China. Environmental Earth Sciences, 80(22): 741. DOI：10.1007/s12665-021-10075-0.

He XD, Li PY, Shi H, et al. 2022. Identifying strontium sources of flowback fluid and groundwater pollution using $^{87}Sr/^{86}Sr$ and geochemical model in Sulige gasfield, China. Chemosphere, 306: 135594. DOI：10.1016/j.chemosphere.2022.135594.

Huang TM, Ma BQ. 2019. The origin of major ions of groundwater in a loess aquifer. Water, 11(12): 2464. DOI：10.3390/w11122464.

Jiang YJ. 2011. Strontium isotope geochemistry of groundwater affected by human activities in Nandong underground river system, China. Applied Geochemistry, 26(3): 371−379. DOI：10.1016/j.apgeochem.2010.12.010.

Jiang YJ, Wu YX, Yuan DX. 2009. Human impacts on Karst groundwater contamination deduced by coupled nitrogen with strontium isotopes in the Nandong Underground River System in Yunan, China. Environmental Science & Technology, 43(20): 7676−7683. DOI：10.1021/es901502t.

Kolodziejska B, Stepień N, Kolmas J. 2021. The influence of strontium on bone tissue metabolism and its application in osteoporosis treatment. International Journal of Molecular Sciences, 22(12): 6564. DOI：10.3390/ijms22126564.

Lebid H, Errih M, Boudjemline D. 2016. Contribution of strontium to the study of groundwater salinity. Case of the alluvial plain of Sidi Bel Abbes (Northwestern Algeria). Environmental Earth Sciences, 75(11): 947. DOI：10.1007/s12665-016-5704-4.

Li XD, Liu CQ, Harue M, et al. 2010. The use of environmental isotopic (C, Sr, S) and hydrochemical tracers to characterize anthropogenic effects on Karst groundwater quality: A case study of the Shuicheng Basin, SW China. Applied Geochemistry, 25(12): 1924−1936. DOI：10.1016/j.apgeochem.2010.10.008.

Li ZB, Huang TM, Ma BQ, et al. 2020. Baseline groundwater quality before shale gas development in Xishui, southwest China: Analyses of hydrochemistry and multiple environmental isotopes (^{2}H, ^{18}O, ^{13}C, $^{87}Sr/^{86}Sr$, ^{11}B, and noble gas isotopes). Water, 12(6): 1741. DOI：10.3390/w12061741.

Liang CC, Wang W, Ke XM, et al. 2022. Hydrochemical characteristics and formation mechanism of strontium-rich groundwater in Tianjiazhai, Fugu, China. Water, 14(12): 1874. DOI：10.3390/w14121874.

Liu D, Tian CJ, Chen XQ, et al. 2023. Insights into

Karst groundwater hydrogeochemical characteristics and spatial evolution in the Jinan Karst aquifer system, Northern China. Water Supply, 23(12): 5004−5016. DOI：10.2166/ws.2023.309.

Liu MJ, Xiao CL, Liang XJ, et al. 2022. Response of groundwater chemical characteristics to land use types and health risk assessment of nitrate in semi-arid areas: A case study of Shuangliao City, Northeast China. Ecotoxicology and Environmental Safety, 236: 113473. DOI：10.1016/j.ecoenv.2022.113473.

Lu SS, Zhou NQ, Jiang SM, et al. 2023. Combining hydrochemistry and environmental isotopes to study hydrogeochemical evolution of Karst groundwater in the Jinci spring area, North China. Carbonates and Evaporites, 38(2): 36. DOI：10.1007/s13146-023-00859-9.

Marie PJ, Ammann P, Boivin G, et al. 2001. Mechanisms of action and TherapeuticPotential of strontium in bone. Calcified Tissue International, 69(3): 121−129. DOI：10.1007/s002230010055.

Musgrove M. 2021. The occurrence and distribution of strontium in U. S. groundwater. Applied Geochemistry, 126: 104867. DOI：10.1016/j.apgeochem.2020.104867.

Négrel P, Petelet-Giraud E. 2005. Strontium isotopes as tracers of groundwater-induced floods: The Somme case study (France). Journal of Hydrology, 305(1−4): 99−119. DOI: 10.1016/j.jhydrol.2004.08.031.

Petelet-Giraud E, Négrel P, Casanova J. 2003. Variability of ^{87}Sr in water draining granite revealed after a double correction for atmospheric and anthropogenic inputs. Hydrological Sciences Journal, 48(5): 729−742. DOI：10.1623/hysj.48.5.729.51448.

Petelet-Giraud E, Négrel P, Gourcy L, et al. 2007. Geochemical and isotopic constraints on groundwater-surface water interactions in a highly anthropized site. The Wolfen/Bitterfeld megasite (Mulde subcatchment, Germany). Environmental Pollution, 148(3): 707−717. DOI：10.1016/j.envpol.2007.01.030.

Pu JB, Yuan DX, Zhang C, et al. 2012. Tracing the sources of strontium in Karst groundwater in Chongqing, China: A combined hydrogeochemical approach and strontium isotope. Environmental Earth Sciences, 67(8): 2371−2381. DOI：10.1007/s12665-012-1683-2.

Qin DJ, Zhao ZF, Guo Y, et al. 2017. Using hydrochemical, stable isotope, and river water recharge data to identify groundwater flow paths in a deeply buried Karst system. Hydrological Processes, 31(24): 4297−4314. DOI：10.1002/hyp.11356.

Raiber M, Webb JA, Bennetts DA. 2009. Strontium isotopes as tracers to delineate aquifer interactions and the influence of rainfall in the basalt Plains of southeastern Australia. Journal of Hydrology, 367(3−4): 188−199. DOI: 10.1016/j.jhydrol.2008.12.020.

Resz MA, Roman C, Senila M, et al. 2023. A comprehensive approach to the chemistry, pollution impact and risk assessment of drinking water sources in a former industrialized area of Romania. Water, 15(6): 1180. DOI：10.3390/w15061180.

Santoni S, Huneau F, Garel E, et al. 2016. Strontium isotopes as tracers of water-rocks interactions, mixing processes and residence time indicator of groundwater within the granite-carbonate coastal aquifer of Bonifacio (Corsica, France). Science of the Total Environment, 573: 233−246. DOI：10.1016/j.scitotenv.2016.08.087.

Schoeller H. 1967. Qualitative evaluation of groundwater resources. In methods and techniques of groundwater investigation and development. UNESCO, Paris: France.

Shoedarto RM, Tada Y, Kashiwaya K, et al. 2021. Investigation of meteoric water and parent fluid mixing in a two-phase geothermal reservoir system using strontium isotope analysis: A case study from Southern Bandung, West Java, Indonesia. Geothermics, 94: 102096. DOI：10.1016/j.geothermics.2021.102096.

Sun XB, Guo CL, Zhang J , et al. 2023. Spatial-temporal difference between nitrate in groundwater and nitrogen in soil based on geostatistical analysis. Journal of Groundwater Science and Engineering, 11(1): 37−46. DOI：10.26599/JGSE.2023.9280004.

Su C, Zhang XQ, Sun YW, et al. 2023. Hydrochemical characteristics and evolution

processes of Karst groundwater in Pingyin Karst groundwater system, North China. Environmental Earth Sciences, 82(2): 67. DOI：10.1007/s12665-022-10717-x.

Ullah Z, Zeng XC, Rashid A, et al. 2023. Integrated approach to hydrogeochemical appraisal of groundwater quality concerning arsenic contamination and its suitability analysis for drinking purposes using water quality index. Scientific Reports, 13: 20455. DOI：10.1038/s41598-023-40105-9.

Wang H, Jiang XW, Wan L, et al. 2015. Hydrogeochemical characterization of groundwater flow systems in the discharge area of a river basin. Journal of Hydrology, 527: 433−441. DOI：10.1016/j.jhydrol.2015.04.063.

Wang YX, Shen ZL, Moisevich SG. 2001. Strontium hydrogeochemistry of thermal groundwaters from Baikal and Xinzhou. Science in China Series E: Technological Sciences, 44(1): 138−143. DOI：10.1007/BF02916805.

Wu WH, Zheng HB, Cao JH, et al. 2014. Sr isotopic characteristics in two small watersheds draining silicate and carbonate rocks: Implication for studies on seawater Sr isotopic evolution. Hydrology and Earth System Sciences, 18(2): 559−573. DOI：10.5194/hess-18-559-2014.

Xiao J, Jin ZD, Wang J. 2014. Assessment of the hydrogeochemistry and groundwater quality of the Tarim River Basin in an extreme arid region, NW China. Environmental Management, 53(1): 135−146. DOI：10.1007/s00267-013-0198-2.

Xie XJ, Wang YX, Ellis A, et al. 2013. Delineation of groundwater flow paths using hydrochemical and strontium isotope composition: A case study in high arsenic aquifer systems of the Datong Basin, Northern China. Journal of Hydrology, 476: 87−96. DOI：10.1016/j.jhydrol.2012.10.016.

Yang N, Su CL, Liu WB, et al. 2022. Occurrences and mechanisms of strontium-rich groundwater in Xinglong County, Northern China: Insight from hydrogeological and hydrogeochemical evidence. Hydrogeology Journal, 30(7): 2043−2057. DOI：10.1007/s10040-022-02533-1.

Yuan JF, Xu F, Deng GS, et al. 2017. Hydrogeochemistry of shallow groundwater in a Karst aquifer system of Bijie city, Guizhou Province. Water, 9(8): 625. DOI：10.3390/w9080625.

Zhang B, Zhao D, Zhou PP, et al. 2020. Hydrochemical characteristics of groundwater and dominant water–rock interactions in the Delingha area, Qaidam Basin, Northwest China. Water, 12(3): 836. DOI：10.3390/w12030836.

Zhang T, Wang P, He J, et al. 2023. Hydrochemical characteristics, water quality, and evolution of groundwater in Northeast China. Water, 15(14): 2669. DOI：10.3390/w15142669.

Zhang Y, Yu S, He SY, et al. 2021. New estimate of chemical weathering rate in Xijiang River Basin based on multi-model. Scientific Reports, 11: 5728. DOI：10.1038/s41598-021-84602-1.

Zieliński M, Dopieralska J, Królikowska-Ciaglo S, et al. 2021. Mapping of spatial variations in Sr isotope signatures ($^{87}Sr/^{86}Sr$) in Poland—Implications of anthropogenic Sr contamination for archaeological provenance and migration research. Science of the Total Environment, 775: 145792. DOI：10.1016/j.scitotenv.2021.145792.